LETTER

Run-and-tumble dynamics of self-propelled particles in confinement

To cite this article: Jens Elgeti and Gerhard Gompper 2015 *EPL* **109** 58003

View the article online for updates and enhancements.

Run-and-tumble dynamics of self-propelled particles in confinement

JENS ELGETI and GERHARD GOMPPER

Theoretical Soft Matter and Biophysics, Institute of Complex Systems and Institute for Advanced Simulation, Forschungszentrum Jülich - 52425 Jülich, Germany

Abstract – Run-and-tumble dynamics is a wide-spread mechanism of swimming bacteria. The accumulation of run-and-tumble microswimmers near impermeable surfaces is studied theoretically and numerically in the low-density limit in two and three spatial dimensions. Both uni-modal and exponential distributions of the run lengths are considered. Constant run lengths lead to peaks and depletions regions in the density distribution of particles near the surface, in contrast to exponentially distributed run lengths. Finally, we present a universal accumulation law for large channel widths, which applies not only to run-and-tumble swimmers, but also to many other kinds of self-propelled particles.

Introduction. – Swimming bacteria like *E. coli* and *Salmonella*, with a body length of just a few micrometers, are too small for spatial sensing of a stimulus gradient along their body size [1,2]. Therefore, they have to resort to temporal sensing, where the gradient is determined along the swimming trajectory. These bacteria have developed a procedure of intriguing simplicity for chemotactic motion —they perform a run-and-tumble motion, in which nearly straight swimming segments are interrupted by tumbling events, where the run length then depends on the sign of the stimulus gradient [1,3]. There is an interesting connection of this run-and-tumble dynamics to Lévy flights [4,5], which suggests that this process could be a very efficient search strategy [6].

For a dilute suspension of microswimmers in a bulk fluid, run-and-tumble dynamics is strictly equivalent to passive-particle diffusion for long times. Here, the diffusion coefficient is given by $D_{eff} = v^2/\tau_r$, where v is the swimming velocity, and τ_r is the run time [7]. The effective diffusion coefficient is typically much larger than the thermal diffusion coefficient. The equivalence also holds in the presence of a slowly varying external potential. This implies that active Brownian particles (ABPs), which display a rotational diffusion instead of tumbling events, are equivalent to run-and-tumble particles (RTPs) under these conditions.

In fact, the equivalence of ABPs and RTPs has been discovered much earlier for the mathematically equivalent case of the conformations of semi-flexible polymers. Here, the worm-like chain model corresponds to ABPs, whereas the freely jointed chain model corresponds to RTPs. The equivalence of the two is expressed by the Kuhn length ξ_K, which is the segment length of the freely jointed chain, to equal twice the persistence length ξ_p of the worm-like chain, such that the end-to-end distance is the same in both descriptions [8].

At higher densities of microswimmers, a density-dependent motility can cause phase separation and accumulation of both RTPs [9–11] and ABPs [12–14], which indicates that the dynamics of active particles is no longer equivalent to passive diffusion. Asymmetric potentials can cause rectification of bacterial motion [7,15,16]. Also, walls and obstacles break the diffusion equivalence, because microswimmers accumulate at walls, in contrast to passive particles. Explanations of this surface trapping usually invoke hydrodynamics [17,18]. Whether it is the detailed hydrodynamics of the corkscrew motion of *E. coli* flagella [19] or the snake-like motion of the sperm tail [20], or the far-field hydrodynamics of a hydrodynamic dipole [17], hydrodynamics provides an effective attraction toward boundaries [18,21,22]. However, for *E. coli*, noise also plays an important role and may even dominate

over the rather weak hydrodynamic interactions [23]. Furthermore, it has been shown that persistent motion drives swimmers to the wall, even in presence of strong orientational fluctuations [24–29]. For harmonic confinement, accumulation away from the center has also been found for run-and-tumble particles [7]. Thus, it is not obvious under which conditions the equivalence between RTPs, ATPs, and passively diffusing particles holds. We want to clarify this question from the point of view of wall accumulation and confinement.

In this letter, we investigate the effect of confinement for particles with a pure run-and-tumble dynamics in the low-density limit and in the absence of hydrodynamic interactions, both analytically and numerically. The structure of the density patterns of RTPs at hard walls is found to depend strongly on the dimensionality of the accessible space —between two planar walls in three dimensions (3D), or along a surface with lateral confinement in two dimensions (2D)— and on the run-length distribution, both quantitatively and qualitatively. Here, the relevant parameter is the dimensionless ratio between channel width and (average) run length, whereas propulsion velocity and tumbling frequency only enter indirectly via the run length. RTPs are predicted to behave quite differently from ABPs. For narrow channels and constant run lengths, the distribution of tumbling events develops pronounced extrema, with a depletion layer near the wall and a maximum at larger distances determined by the run length. These structures disappear for exponentially distributed run lengths. Thus, the behavior depends sensitively on the run-length distribution. In contrast, for wide channels, we predict a (nearly) universal wall-accumulation law for self-propelled particles. This wall-accumulation law only relies on symmetries and dimensional arguments, and thus holds for many different types of microscopic swimmers.

Wild-type *E. coli* have an average run length of $12\,\mu\text{m}$ [30], which is the same order of magnitude as the channel width of microfluidic devices used to manipulate and study these bacteria [31–33]. Therefore, our results are relevant, *inter alia*, for the design of microfluidic devices for rectification and sorting of run-and-tumble bacteria.

Model and simulation technique. – We study run-and-tumble dynamics of individual microswimmers in confinement. A particle performs a forward run with a velocity v for a time τ_r. Each run is followed by a tumble event, where a new orientation angle θ (see fig. 1) is chosen randomly on the unit circle (2D) or unit sphere (3D), *i.e.* there is no memory of the orientation before the tumbling event. The particle coordinate z perpendicular to the wall is then updated by $z(t + \tau_r) = z(t) + \cos(\theta)L$. Here, the run length $L = v\tau_r$ is either constant, or drawn from an exponential distribution depending on the dynamics studied. It is important to note that properties of RTPs do not depend on v and τ_r separately, but only on the run length. Due to symmetry, motion parallel to the wall does
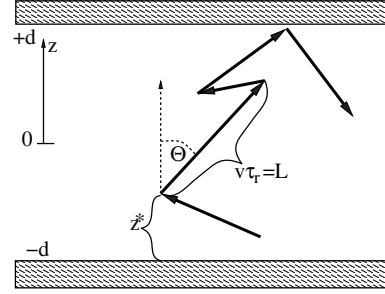

Fig. 1: Schematic of run-and-tumble dynamics. A "run" of the particle with a velocity v for a time τ_r is followed by a tumbling event, resulting in a new orientation θ. The particle is confined between two parallel walls at $z = \pm d$. z^* denotes the distance from the walls.
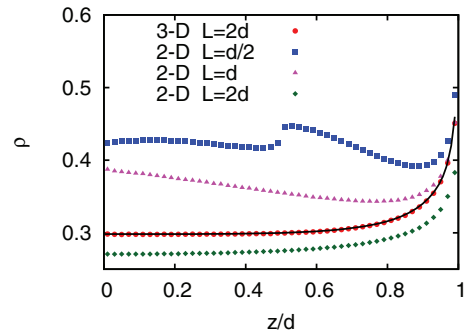

Fig. 2: (Colour on-line) Particle density distribution $\rho(z)$ for various run lengths L. The solid line is the exact analytic solution (19) for the particle density in three dimensions for run lengths larger than the channel width $2d$.

not have to be considered. If the particle hits a wall, it remains there —possibly sliding parallel to the wall— until the next tumbling event occurs. After a sufficiently long equilibration time, the probability density to find the particle at a position z is recorded by a histogram over 10^8 to 10^9 tumbling steps. A few examples of density distributions for various run lengths are shown in fig. 2.

The trajectory of an RTP is completely defined by the location of the tumbling events, since the motion between these events is just ballistic. This implies, in particular, that no orientation vector of the particle is needed to describe the dynamics. Thus, the continuous-time dynamics of a RTP in three spatial and two orientational dimensions is mapped onto a discrete-time-step model in one spatial dimension. Physically and mathematically, the fundamental quantity to compute in the steady state is then the tumbling density $\phi(z)$. The particle density $\rho(z)$ then follows from $\phi(z)$ by a convolution, as explained in detail below. Both densities are directly asccessible experimentally; however, the tumbling density is more difficult to measure, because the trajectories of (all) particles have to be traced.

Thus, we first focus on the more fundamental tumbling density, which is the (normalized) probability to find a

tumbling event at a position z. The mirror symmetry of the system is reflected in the symmetry of the tumbling density, $\phi(z) = \phi(-z)$. The time evolution of the tumbling density is determined by

$$\phi(z, t + \tau_r) = \int_{-d}^{+d} \phi(z', t) p(z - z') \mathrm{d}z'. \qquad (1)$$

Here, $p(\Delta z)$ is the transfer function of particles moving to a new position, which depends implicitly on the run-length distribution. It is the number of orientational microstates of an unconfined particle which are compatibe with a given Δz-displacement. This probability density depends on the dimensionality of the system, and on the run-length distribution (unimodal or exponentially distributed). At the walls, particles accumulate in a δ-distribution because all particles that hit the wall are located there. Thus, we have the boundary conditions

$$\phi(\pm d, t) = 0.5 \phi_s(t) \delta(z \pm d) \qquad (2)$$

$$0.5 \phi_s(t + \tau_r) = \int_{-d}^{d} \phi(z', t) P(-z' - d) \mathrm{d}z', \qquad (3)$$

where ϕ_s is the probability to find a tumbling event at the wall, and P is the cumulative distribution function of p, i.e. $P(z) = \int_{-\infty}^{z} p(z') \mathrm{d}z'$.

Constant run lengths. – We begin our analysis in the simplest case of constant run length L. The transfer function is discontinuous at the run length, as runs longer than L cannot occur. In three dimensions, the transfer function $p(z)\mathrm{d}z$ is obtained by an integral over the surface of a sphere of radius L with values of the vertical displacement between z and $z + \mathrm{d}z$. This yields immediately that the transfer function is

$$p_{(3,c)}(z) = \frac{1}{2L} \Theta(L - z) \Theta(L + z), \qquad (4)$$

where $\Theta(z)$ is the Heaviside step function. Subscripts denote dimensionality and the type of run-length distribution ($c = $ constant, $e = $ exponential). Similarly, in two dimensions, integration over a circle of radius L with displacement between z and $z + \mathrm{d}z$ yields even a divergence of the transfer funtion at the run length,

$$p_{(2,c)}(z) = \frac{1}{\pi L \sqrt{1 - (z/L)^2}} \Theta(L - z) \Theta(L + z). \qquad (5)$$

The simplicity of the 3D transfer function allows for an analytic solution for narrow channels with $2d < L$,

$$\phi_{(3,c)}(z) = \frac{1}{2L} + \frac{1 - d/L}{2} [\delta(z - d) + \delta(z + d)]. \qquad (6)$$

In 2D, an analytical solution can only be obtained by assuming that the number of tumbling events in the bulk is negligible compared to tumbling events at the wall (i.e. $\int_{-d+\epsilon}^{d-\epsilon} \phi(z) \mathrm{d}z \ll \phi_s$ with an infinitesimal length ϵ).

This results in

$$\phi_{(2,c)}(z) = \frac{\pi}{\pi + \sin^{-1}(2d/L)} [0.5\delta(z - d) + 0.5\delta(z + d)]$$

$$+ \frac{1}{2\pi + 2\pi \sin^{-1}(2d/L)}$$

$$\times \left[\frac{1}{\sqrt{L^2 - (z - d)^2}} + \frac{1}{\sqrt{L^2 - (z + d)^2}} \right]. \qquad (7)$$

These analytical results and corresponding simulation data are displayed in fig. 3. The comparison shows that the solution (6) in 3D and the approximate expression (7) in 2D work very well for the appropriate regimes. Figure 3 reveals that the walls induce a very rich structure of the tumbling density in the channel for $2d \geq L$, i.e. for channels wider than the run length. The density profiles all collapse onto a single master curve when the tumbling density is scaled by the bulk density ϕ_b (the density far away from the wall) and distances are scaled by the run length. In this case, the high particle density at the walls generates depletion regions near the walls, and two pronounced peaks at a distance L from the wall, which can easily be recognized in fig. 3 (middle) and (right). In 2D, these primary peaks generate secondary peaks for $d \geq L$, which are again displaced by a distance L further away from wall they first came from. In 3D, the primary singularities are too weak to generate visible secondary peaks. All bulk singularities disappear for $L > 2d$, compare eq. (6), because particles can move directly from one wall to the other in a single step. These depletion zones and peaks can be understood by starting from a uniform bulk distribution plus δ-peaks at the walls, and iterating eq. (1) once, as explained in more detail below.

Exponential run-length distribution. – In the case of a distribution of run lengths, the transfer functions are obtained by convolution of the (conditional) probabilities $p(z|L')$ —resulting from step with run length L'— with the run-length distribution $p_{len}(L')$, i.e.

$$p_{(n,len)}(z) = \int_{z}^{\infty} P_{(n,c)}(z|L') p_{len}(L') \mathrm{d}L'. \qquad (8)$$

The integral has a lower boundary at z, because $\Delta z = z$ cannot be achieved with $L' < z$.

We focus here on exponential run-length distributions,

$$p_{len}(L') = \lambda \exp(-\lambda L'), \qquad (9)$$

with $\langle L' \rangle \equiv L = 1/\lambda$, which mimic the run-length distribution of *E. coli*. This yields the transfer functions

$$p_{(2,e)}(z) = \frac{1}{\pi L} K_0 \left(\frac{|z|}{L} \right),$$

$$p_{(3,e)}(z) = \frac{1}{2L} E_1 \left(\frac{|z|}{L} \right) \qquad (10)$$

with K_0 a Bessel function and E_1 an exponential-integral function. The continuity and strong decay of these transfer functions lead to the disappearance of all the singularities of the tumbling density found for constant run length,
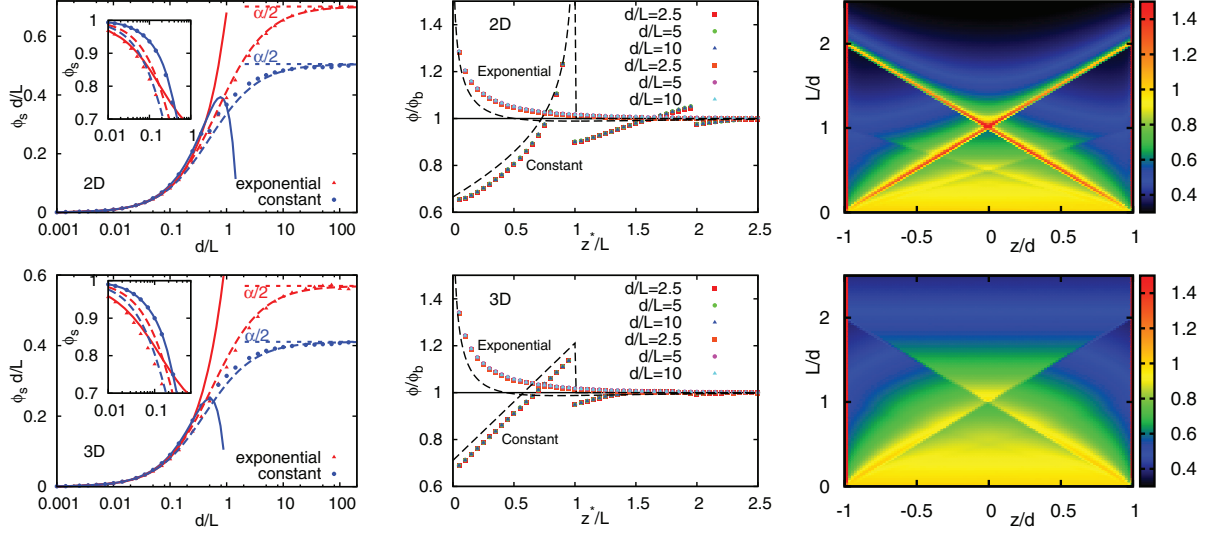
Fig. 3: (Colour on-line) Tumbling density profiles $\phi(z)$ for (top) two and (bottom) three dimensions. Left: scaled surface density $\phi_s d/L$ as a function of the ratio d/L of channel width and run length. Solid lines are analytical approximations for narrow channels (see text), dashed lines are fits to the large-channel approximation (14). Note that for $d \gg L$, ($\phi_s d/L$) approaches $\alpha/2$. Middle: scaled tumbling density $\phi(z^*)/\phi_b$ as a function of the scaled distance $z^*/L = (z + d)/L$ from the wall. Dashed lines show the approximation $\phi_1(z^*)$, which is obtained from a first-order iteration of eq. (1) (see text). Right: density of tumbling events $\phi(z/L)$ inside the channel for various (constant) run lengths. For $2d \geq L$, the presence of the two walls induces strong density modulations.

see fig. 3. Thus, the tumbling density is highly sensitive to the run-length distribution.

We estimate the density profile in small channels, by neglecting the particles in the bulk in eq. (1), as for constant run length. In two and three spatial dimensions, we then obtain

$$\phi_{s(2,e)} = [1 + \lambda d K_0(2\lambda d) L_{-1}(2\lambda d) \\ + \lambda d K_1(2\lambda d) L_0(2\lambda d)]^{-1}, \qquad (11)$$

$$\phi_{s(3,e)} = \left[1 + \frac{1 - E_2(2\lambda d)}{2}\right]^{-1}, \qquad (12)$$

where the $L_i(x)$ with $i = -1, 0$ are Struve functions, and $E_i(x)$ with $i = 1, 2$ are exponential-integral functions. Figure 3 demonstrates that these approximations work very well for narrow channels. However, the critical length scale, where they break down, is significantly lower than for constant run length. The reason is that the transfer functions for exponentially distributed run lengths decay much faster than the transfer functions for constant run lengths. This implies that there are more particles inside the channel, so that the approximation $\int_{-d+\epsilon}^{d-\epsilon} \phi(z)\mathrm{d}z \ll \phi_s$ breaks down already at smaller channel widths.

Scaling behavior of wall density. – For channels much wider than the (average) run length, we can use scaling arguments to determine the wall accumulation of particles. For $d \gg L$, the tumbling density profile eventually becomes flat far from the walls. Everything else fixed, the surface density has to be linear in the bulk density ϕ_b defined as the (constant) density far from the walls. Since the (average) run length L is the only relevant length scale near the wall, the proportionality factor has to be linear in L, so that[1]

$$\phi_s = \alpha L \phi_b \qquad (13)$$

with a dimensionless prefactor α. In a channel of finite width d, normalization then gives

$$\phi_s = \frac{\alpha L}{\alpha L + 2d} = \frac{1}{1 + 2d/(\alpha L)}. \qquad (14)$$

The surface accumulation factor α is independent of the run length, and only depends on the dynamics (*i.e.* 2D/3D, constant run length/exponential run-length distribution). From our simulations, we obtain the accumulation factors shown in table 1. The large-distance approximation (14) works very well for $d > L$, and even for smaller channels it is not too far off (see fig. 3). Uni-modal and exponential run-length distributions result in accumulation factors α, which are clearly different, but still of the same order of magnitude. Thus, measurements of $\alpha \equiv \phi_s/(L\phi_b)$ for $d \gg L$ might provide a new possibility to characterize run-length distributions experimentally.

---

[1]Alternatively, it can be argued that the surface density ϕ_s, which is dimensionless in our description, can only depend on the ratio of the two available length scales L and d, which implies $\phi_s = F(d/L)$, with some unknown scaling function $F(x)$. This can also be seen by considering an infinite half-space, with a wall at $z = 0$. In this case, the boundary condition is that the density approaches ϕ_b for $z \to \infty$. Then, L is the only available length scale. For finite but very wide channel, the density profile should not change. However, the normalization of the probability density introduces a constraint on ϕ_b, which implies $\phi_b \sim 1/d$.

Table 1: Accumulation factor α for various self-propelled particles in two and three spatial dimensions. For ABPs, α-values are obtained from direct Langevin simulations; in this case, we employ the "Kuhn" length as the characteristic length scale.

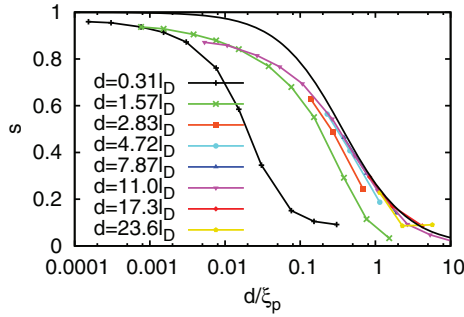| α	2D	3D
RTPs, constant L	1.01(2)	0.82(2)
RTPs, exponential L' distr.	1.40(2)	1.14(2)
ABPs, $L = 2\xi_p$	0.80(3)	0.37(3)

Fig. 4: (Colour on-line) Surface excess $s = \int(\rho(z) - \rho_b)\mathrm{d}z$ for self-propelled Brownian spheres. Data from ref. [26]. Here, s is to be considered equivalent to ϕ_s. The wide-channel approximation (14) works already rather well for channels widths $2d$ comparable to the persistence length ξ_p, as long as ξ_p is much larger than the diffusive length scale $l_D = \sqrt{D_t/D_r}$.

Since these arguments rely only on dimensional analysis, the results should be valid for other types of self-propelled particles as well (as long as there is one dominant length scale of the dynamics). For active Brownian spheres, this length scale is the persistence length of the trajectory $\xi_p = v/D_r$, where D_r is the rotational diffusion coefficient. Using data from ref. [26], we find indeed an excellent agreement for channels much larger than the diffusive length scale $l_D = \sqrt{D_t/D_r}$, where D_t is the translational diffusion coefficient (see fig. 4). Note that eq. (14) also predicts a crossover from narrow- to wide-channel behavior at $L \simeq 2d$ for all kinds of self-propelled particles. The fact that the α-values in table 1 differ significantly for RTPs and ABPs clearly demonstrates that these two types of self-propelled motion are *not* equivalent near surfaces. However, the fact that these factors are all of order unity emphasizes the generic aspect of wall accumulation.

Near-wall density in wide channels. – For wider channels, the surface density ϕ_s is well described by eq. (14). To understand the structure of the density distribution close to the wall, the stationary form of eqs. (1) to (3) can be used to obtain an analytical approximation. We start as an initial guess with a δ-distribution at the wall, with an amplitude ϕ_s, plus a constant tumbling density ϕ_b in the bulk (see eq. (14)). An iteration with eq. (1)

then yields

$$\phi_1(z^*) = \frac{\phi_s}{4}\delta(z^*) + \phi_b\delta(z^*)\int_0^\infty P(z')\mathrm{d}z'$$
$$+ \frac{\phi_s}{2}p(z^*) + \phi_b\left(1 - \int_\infty^0 p(z^* - z')\mathrm{d}z'\right). \quad (15)$$

Note that the last two terms on the right-hand side of eq. (15) determine the spatial dependence of the tumbling density near the wall. Figure 3 (middle) shows that this first-order calculation can qualitatively explain the numerical results for the structure of the tumbling density profile. In particular, for constant run lengths, it reproduces and explains the near-wall dip in the tumbling density, *i.e.* the formation of a depletion layer close to the wall, and in turn a peak and discontinuity at $z = L$. As shown in fig. 3 (right), this peak leads to interesting patterns in the tumbling density distribution for channel widths larger than the run length, in particular a very pronounced peak in the channel center for $d = L$.

Microswimmer density. – Finally, we connect the tumbling density to the number density of microswimmers. This requires the convolution of the tumbling density with the spreading function $f(\Delta z)$ of one run,

$$\rho(z) = \int_{-\infty}^\infty \phi(z')f(z - z')\mathrm{d}z' \quad (16)$$

(where the particles which would penetrate the walls have to be "folded back" to the wall, *i.e.* $\phi_s(d) = \int_d^\infty P(z)\mathrm{d}z$). For constant run length, the spreading function $f(\Delta z)$ is obtained from the transfer functions as

$$f(z) = \int_z^\infty \frac{p(z')}{z'}\mathrm{d}z', \qquad \text{for} \quad z > 0, \quad (17)$$

and $z < 0$ follows from symmetry[2]. Note that if the tumbling time τ_t cannot be neglected compared to the run time τ_r, the tumbling density has to be added proportional to τ_t/τ_r in eq. (16). As an example, we consider here the case of thin three-dimensional channels ($2d < L$) and constant run length, which can be solved analytically. Here, the spreading function is found to be

$$f(z) = \frac{1}{2L}\ln\left(\frac{L}{|z|}\right), \quad (18)$$

which yields the particle density (for $z > 0$)

$$\rho(z) = \frac{1}{4L}\left[\ln\left(\frac{L}{d+z}\right) + \ln\left(\frac{L}{d-z}\right)\right]$$
$$+ \frac{d}{4L^2}\left[2 + \frac{z}{d}\ln\left(\frac{d-z}{d+z}\right)\right]$$
$$+ \frac{\rho_s}{2}\delta(z - d) + \frac{\rho_s}{2}\delta(z + d), \quad (19)$$

where the surface density ρ_s of particles is obtained from the normalization condition. Equation (19) fits the simulations perfectly, without any adjustable parameters, see fig. 2.

---

[2]In the more general case, eq. (17) has to be modified to account for the run-length distribution.

Conclusions. – We have shown that run-and-tumble dynamics of self-propelled particles leads to highly structured density distributions near impenetrable surfaces. Due to the absence of translational diffusion, accumulation materializes in the form of δ-function peaks at the surface. Diffusion would broaden these peaks, similarly as predicted for ABPs [26]. Close to confining walls, RTPs are thus clearly not equivalent to either diffusing particles or ABPs. The density distributions are predicted to depend sensitively on the spatial dimensionality and on the run-length distribution, where the typical length scale is set by the (average) run length.

While the dynamics considered here is certainly oversimplified for real microswimmers like *E. coli*, it captures the essential aspects of run-and-tumble motion, and similar results can be expected for other types of Lévy flights. In particular, the limit of large wall separations for the accumulation is very generic, and should thus apply to many systems of self-propelled particles and microswimmers [21,22]. It will be interesting to see whether this behavior extends to systems in which hydrodynamic interactions play a significant role.

Another interesting issue is the behavior of RTPs at finite particle density [9–11]. For high density, the characteristic features in confinement revealed by our study will almost certainly be washed out, because collisions will dominate over tumbling events. However, interesting behavior can be expected in confinement, when the average distance between particles becomes comparable with the run length.

REFERENCES

[1] BERG H. C. and PURCELL E. M., *Biophys. J.*, **20** (1977) 193.
[2] DUSENBERY D. B., *Biophys. J.*, **74** (1997) 2272.
[3] BERG H. C., *E. coli in Motion* (Springer, New York) 2004.
[4] THIEL F., SCHIMANSKY-GEIER L. and SOKOLOV I. M., *Phys. Rev. E*, **86** (2012) 021117.
[5] ANGELANI L., *EPL*, **102** (2013) 20004.
[6] LOMHOLT M. A., KOREN T., METZLER R. and KLAFTER J., *Proc. Natl. Acad. Sci. U.S.A.*, **105** (2008) 11055.
[7] TAILLEUR J. and CATES M. E., *EPL*, **86** (2009) 60002.
[8] RUBINSTEIN M. and COLBY R. H., *Polymer Physics* (Oxford University Press, USA) 2003.
[9] CATES M. E. and TAILLEUR J., *EPL*, **101** (2013) 20010.
[10] PAOLUZZI M., DI LEONARDO R. and ANGELANI L., *J. Phys.: Condens. Matter*, **25** (2013) 415102.
[11] SOTO R. and GOLESTANIAN R., *Phys. Rev. E*, **89** (2014) 012706.
[12] FILY Y. and MARCHETTI M. C., *Phys. Rev. Lett.*, **108** (2012) 235702.
[13] WYSOCKI A., WINKLER R. G. and GOMPPER G., *EPL*, **105** (2014) 48004.
[14] STENHAMMAR J., MARENDUZZO D., ALLEN R. J. and CATES M. E., *Soft Matter*, **10** (2014) 1489.
[15] KOUMAKIS N., LEPORE A., MAGGI C. and LEONARDO R. D., *Nat. Commun.*, **4** (2013) 2588.
[16] BERDAKIN I., JEYARAM Y., MOSHCHALKOV V. V., VENKEN L., DIERCKX S., VANDERLEYDEN S. J., SILHANEK A. V., CONDAT C. A. and MARCONI V. I., *Phys. Rev. E*, **87** (2013) 052702.
[17] BERKE A. P., TURNER L., BERG H. C. and LAUGA E., *Phys. Rev. Lett.*, **101** (2008) 038102.
[18] SPAGNOLIE S. E. and LAUGA E., *J. Fluid Mech.*, **700** (2012) 105.
[19] LAUGA E., DILUZIO W. R., WHITESIDES G. M. and STONE H. A., *Biophys. J.*, **90** (2006) 400.
[20] ELGETI J., KAUPP U. B. and GOMPPER G., *Biophys. J.*, **99** (2010) 1018.
[21] LAUGA E. and POWERS T. R., *Rep. Prog. Phys.*, **72** (2009) 096601.
[22] ELGETI J., WINKLER R. G. and GOMPPER G., to be published in *Rep. Prog. Phys.* (2015), arXiv:1412.2692.
[23] DRESCHER K., DUNKEL J., CISNEROS L. H., GANGULY S. and GOLDSTEIN R. E., *Proc. Natl. Acad. Sci. U.S.A.*, **108** (2011) 10940.
[24] ELGETI J. and GOMPPER G., *EPL*, **85** (2009) 38002.
[25] LI G. and TANG J. X., *Phys. Rev. Lett.*, **103** (2009) 078101.
[26] ELGETI J. and GOMPPER G., *EPL*, **101** (2013) 48003.
[27] FILY Y., BASKARAN A. and HAGAN M. F., *Soft Matter*, **10** (2014) 5609.
[28] COSTANZO A., ELGETI J., AUTH T., GOMPPER G. and RIPOLL M., *EPL*, **107** (2014) 36003.
[29] YANG X., MANNING M. L. and MARCHETTI M. C., *Soft Matter*, **10** (2014) 6477.
[30] BERG H. and BROWN D., *Nature*, **239** (1972) 500.
[31] DILUZIO W. R., TURNER L., MAYER M., GARSTECKI P., WEIBEL D. B., BERG H. C. and WHITESIDES G. M., *Nature*, **435** (2005) 1271.
[32] HULME S. E., DILUZIO W. R., SHEVKOPLYAS S. S., TURNER L., MAYER M., BERG H. C. and WHITESIDES G. M., *Lab Chip*, **8** (2008) 1888.
[33] BERDAKIN I., SILHANEK A. V., MOYANO CORTEZ H. N., MARCONI V. I. and CONDAT C. A., *Cent. Eur. J. Phys.*, **11** (2013) 1653.